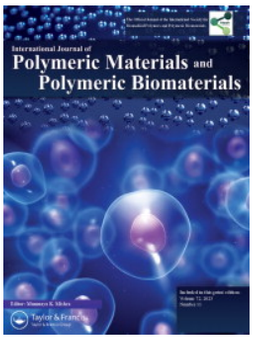

International Journal of Polymeric Materials and Polymeric Biomaterials

ISSN: (Print) (Online) Journal homepage: https://www.tandfonline.com/loi/gpom20

Gentamicin and fluconazole loaded electrospun polymethylmethacrylate (PMMA) fibers as a novel platform for the treatment of corneal keratitis

Oguzhan Gunduz & Songul Ulag

To cite this article: Oguzhan Gunduz & Songul Ulag (2022): Gentamicin and fluconazole loaded electrospun polymethylmethacrylate (PMMA) fibers as a novel platform for the treatment of corneal keratitis, International Journal of Polymeric Materials and Polymeric Biomaterials, DOI: 10.1080/00914037.2022.2071271

To link to this article: https://doi.org/10.1080/00914037.2022.2071271

Published online: 06 May 2022.

INTERNATIONAL JOURNAL OF POLYMERIC MATERIALS AND POLYMERIC BIOMATERIALS
https://doi.org/10.1080/00914037.2022.2071271

Gentamicin and fluconazole loaded electrospun polymethylmethacrylate (PMMA) fibers as a novel platform for the treatment of corneal keratitis

Oguzhan Gunduz[a,b] and Songul Ulag[a,b]

[a]Center for Nanotechnology & Biomaterials Application and Research (NBUAM), Marmara University, Istanbul, Turkey; [b]Department of Metallurgical and Materials Engineering, Faculty of Technology, Marmara University, Istanbul, Turkey

ABSTRACT

In this study, 10 mg fluconazole (10 FCZ) and 10 mg gentamicin (10 GEN) loaded with 40% polymethylmethacrylate (40% PMMA) fibers were fabricated by electrospinning and the performance of the formulations (40% PMMA, 40% PMMA/10 FCZ, 40% PMMA/10 GEN, and 40% PMMA/10 FCZ/10 GEN) was tested. 10 mg Gentamicin-loaded 40% PMMA fiber mat showed a more significant zone of inhibition against the *S. aureus* compared to the zone of 40% PMMA/10 GEN/10 FCZ fiber. The biocompatibility test using a human adipose-derived mesenchymal stem cell (MSCs) as a cell model proved that the amount of loaded and released GEN has no toxic effects on the MSCs.

GRAPHICAL ABSTRACT

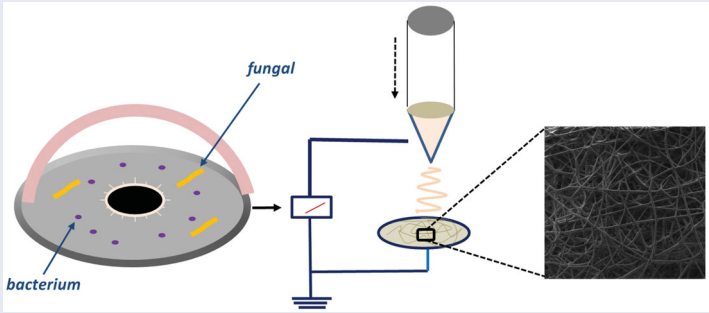

ARTICLE HISTORY
Received 9 March 2022
Accepted 25 April 2022

KEYWORDS
Corneal keratitis; electrospinning; fiber

1. Introduction

Corneal keratitis is an ocular infectious disease caused by microorganisms and can threaten vision[1]. It can be occurred by bacteria, fungi, viruses, or protozoa. However, the microorganisms that cause vision-threatening keratitis are bacteria. Gram-negative or gram-positive bacteria can be responsible for this infectious disease. It is a crucial infection originating from the cornea and is one of the most common causes of definitive blindness in the world[2]. The course of the disease may vary depending on the pathogenicity of the bacteria causing the infection and the condition of the cornea[3,4]. Along with geographical and climatic factors, increasing contact lenses, ocular trauma, or ocular surface diseases have caused corneal keratitis in recent years[5,6]. It may also occur as a post-transplant complication[7]. It is defined by white and yellowish fluids in the corneal stroma region, independent of the presence of an epithelial defect in the cornea[8]. The eyelids and tear film protect the cornea against pathogens. In addition, passive and active host defense mechanisms also protect the cornea from bacteria. However, if the defendant fails or the corneal epithelium is damaged, the bacteria damage the cornea[9,10]. It may recur at certain intervals. Dry eye syndrome or eyelid abnormalities are causes of these recurrences[11]. With early diagnosis and prompt treatment, structural damage to the cornea can be reduced, and vision loss can be prevented. Some signs and symptoms of corneal keratitis are as follows: lid and conjunctival edema decreased vision, pain, redness, photophobia, and discharge. The degree of these signs and symptoms depends on factors such as the virulence of the organism, whether there is previous damage to the cornea, and how long the infection has lasted[2]. Complete healing may not be possible in corneal keratitis. After treatment, problems in vision and lack of vascularization may occur[12]. Bacterial keratitis is the most harmful corneal keratitis caused by microorganisms. Any corneal keratitis should be treated as bacterial keratitis unless proven otherwise. No single antibiotic is the solution to treating corneal keratitis caused by bacteria[2]. Pathogens causing corneal keratitis are mostly *Staphylococcus aureus*, *Streptococcus pneumonia*, *Serratia,* and *Pseudomonas* species[13]. It has been stated in previous studies that corneal keratitis is usually caused by

CONTACT Oguzhan Gunduz ucemogu@ucl.ac.uk Center for Nanotechnology & Biomaterials Application and Research (NBUAM), Marmara University, Istanbul, Turkey.

more than one bacteria[14]. In recent years, amniotic membrane (AM) transplantation has been used to treat various ocular surface diseases, but AM transplantation has negative aspects related to surgical procedures[15]. Another potential approach to treating corneal keratitis is administering an anti-scarring agent and an antibiotic incorporated into a dosage form[16]. Nanofibrous structures can be fabricated using various techniques and provide the advantage of a high surface-to-volume ratio. The fabrication of biocompatible nanofiber materials for wound treatment can be accomplished by electrospinning[17]. The high surface/volume ratio of nanofiber structures positively affects the adhesion and spread of cells. A large surface area prevents liquid accumulation and facilitates gas passage[18]. The most significant advantage of electrospinning is that electrospun fibers can prolong the release of drugs and act locally, compared to drugs in solution form[16].

PMMA is compatible with human tissue and is used in many applications such as polymer electrolytes, polymer viscosity, and drug delivery using electro-diffusion or electro-osmotic flow[19,20]. It is also widely used in biomedical applications due to its non-toxicity, less cost, biocompatibility, and low probability of inflammatory response when interacting with tissue. In additive surgery, it is generally used to treat both laser-assisted in situ keratomileusis and post-keratoconus corneal ectasia[21]. In addition, PMMA prolongs the biodegradability of the material. In this study, both FCZ and GEN (10 mg) were added separately into the 40% PMMA matrix, and then both of them were loaded in the 40% PMMA. The aim is to provide the antibacterial activity of both gram-positive and gram-negative bacteria by combining these two drugs. GEN is an antibiotic effective against gram-negative bacteria and FCZ is an antibiotic effective against gram-positive bacteria. FCZ is also effective for some fungal strains. Therefore, the fabricated electrospun fiber mat was also tested with fungal strains. This study aims to produce a fiber patch effective against both gram-negative and gram-positive bacteria for the solution of corneal keratitis.

2. Materials and methods

2.1. Materials

Polymethyl methacrylate (MW $= 12 \times 10^4$ g/mol) was bought from Sigma Aldrich, USA. Dimethylformamide (DMF) and Tetrahydrofuran (THF) were supplied from Merck KGaA, Germany. Fluconazole (MW = 306.27 g/mol) was bought from Supelco® Analytical Products Merck, KGaA, Germany. Gentamycin Sulfate (potency: >590 µg/mg) was obtained by BioShop, Canada.

2.2. Preparation of the solutions

Firstly, 40% PMMA was put in 20 mL DCM: THF (50: 50) anhydrous solvent mixture and waited for complete dissolution at room temperature for 3 hours using a magnetic stirrer. Then, 10 mg FCZ and 10 mg GEN were added into the 40% PMMA matrix separately and together to reinforce the antimicrobial and biocompatibility properties of the 40% PMMA matrix. As a result, the final formulations were 40% PMMA, 40% PMMA/10FCZ, 40% PMMA/10GEN, and 40% PMMA/10FCZ/10GEN. To decrease the surface tension, 3% Tween 80 (Merck KGaA, 64271, Germany) was added to these solutions and stirred for 15 min at the magnetic stirrer. Firstly, 40% PMMA was dissolved in the solvent mixture, and then 3% Tween 80 was added into this solution and stirred for 15 min at the magnetic stirrer. After 15 min, 10 mg FCZ, 10 mg GEN, and 10 mg FCZ and GEN were added into this matrix solution (40% PMMA) separately. After drugs were completely dissolved, they were prepared for electrospinning.

2.3. Electrospinning process and physical characterizations of the solutions

After the preparations of the solutions, they were electrospinning to fabricate a fiber mat. During the electrospinning, voltage, flow rate, and distance between the collector and needle were adjusted due to the physical properties of the solutions. A syringe pump (NE-300, New Era Pump Inc., USA), a single brass needle (outer diameter: 1.63 mm), power supply were utilized with a laboratory-scale electrospinning machine (Tribot, Istanbul, Turkey). As a first step, 10 ml of plastic syringes were used to put the solutions. Then, the voltage was applied to form the Taylor cone. The optimized electrospinning parameters obtained in this study were 25–26.5 kV voltage range, 2–3 ml/h flow rate, and 12 cm distance. After fabricating the fiber mat, they were put in + 4 °C overnight. Since the drugs had +4 °C storage conditions, the drug-loaded fibers were also stored at +4 °C.

2.4. Characterization of the electrospun fiber mat

2.4.1. Morphological analysis by SEM

Morphological properties of the fiber mat were determined using a scanning electron microscope (SEM, MA-EVO10, ZEISS) under 23 °C, 50% relative humidity, and 20 kV vacuum. 50 fibers in the SEM images were selected and measured with the Image-J program[22]. The mean and standard deviation values belonged to the measurements of these 50 fibers for each mat.

2.4.2. Fourier transform infrared spectroscopy (FT-IR) analysis

The physicochemical possessions of the fiber scaffolds were observed with Fourier transform infrared spectroscopy (FT-IR, JASCO-4000) at a 4000–400 cm^{-1} scanning range.

2.4.3. Investigations of the thermal properties of the fiber mat

2.4.3.1. Differential scanning calorimetry (DSC). Differential scanning calorimetry (DSC, DSC-60 Plus, Shimadzu) was used to observe the thermal properties of the fiber mat. The

process parameters were adjusted to a 25–200 °C temperature range and 10 °C/min heating rate.

2.4.3.2. Thermogravimetric analysis (TGA). Thermogr avimetric Analyzer (STA-7200) was used to observe the thermal stability of the fiber mat. In this test, nearly 0.2-1 mg fibers were placed in a platinum pan, and nitrogen was utilized to get an inert atmosphere. The temperature range was adjusted from 25 °C to 700 °C with a constant heating rate of 20 °C per minute.

2.4.4. Tensile testing

The mechanical properties of the fiber mat were determined with the uniaxial tensile testing (Shimadzu EZ-LX) device. The test speed was adjusted to 5 mm/min during the test. Three mats with an average height of 50 mm, a width of 10 mm, and a thickness of 0.1 mm were used for all formulations, and they were put directly between the jaws in the device.

2.4.5. Assessment of antimicrobial activity

Staphylococcus aureus ATCC 29213 and *P. aeruginosa* ATCC 27853 were cultured on Columbia Agar and McConkey agar media with 5% sheep blood, respectively, the day before. It was incubated overnight at 35 °C. Bacterial suspensions were prepared in Mueller Hinton Broth (MHB; Biomerieux, France) with a turbidity of 0.5 McFarland ($1–5 \times 10^8$ CFU/mL). The suspensions were spread to cover the entire surface of Mueller Hinton E Agar (MHE; Biomerieux, France) medium. The disks, which had been sterilized under UV light overnight, were placed on the medium at an equal distance. Disks containing 30 µg amikacin were used for both bacteria as control antibiotics. The media were incubated for 16–20 hours at 37 °C. After incubation, the zone diameter of growth inhibition around the disk was determined in mm. *S. pneumoniae* ATCC 49619 was inoculated on Columbia Agar medium with 5% sheep blood. It was incubated overnight at 35 °C in a 5% CO_2 oven. A suspension of bacteria was prepared at a turbidity of 0.5 MacFarland ($1–5 \times 10^8$ CFU/mL) in MHB. The suspension was seeded in Muller Hinton F agar (MHF; Biomerieux, France) medium to cover the entire surface. Disks were placed on the medium at equal intervals. A disk containing 10 µg norfloxacin was used as a control antibiotic. The media were incubated for 16–20 hours in an oven with 5% CO_2 at ∼35 °C. After incubation, the zone diameter of growth inhibition around the disk was measured in mm. *C. parapsilosis* ATCC 22019 and *C. albicans* SC5314 were incubated overnight in Saboraud dextrose agar (SDA, Biomerieux, France) medium and an oven at 30 °C. A suspension of 0.5 MacFarland ($1–5 \times 10^6$ CFU/mL) turbidity in physiological saline was prepared with the growing colonies. Fungal suspensions were spread on 2 separate MHE agar media. The disks were placed at an equal distance. A 70% ethanol impregnated disk was used as the control disk. It was incubated for 20–24 hours at 35 °C. After incubation, the zone diameter of growth inhibition around the disk was determined by measuring in mm. In addition, all disks were placed in a sterile MHE agar medium for contamination evaluation during the study. The presence of growth around the disk was examined for contamination analysis.

2.4.6. Biocompatibility test

To examine the biostability properties of the electrospun fiber mat, a human adipose-derived mesenchymal stem cell line (American Type Culture Collection (ATCC, ATCC-PCS-500-011) was used. In the MTT assay, mesenchymal stem cells were incubated with Dulbecco's Modified Eagles Medium (DMEM) which was supplemented with 1% penicillin-streptomycin (Invitrogen) and 10% fetal bovine serum (FBS, Invitrogen). The scaffolds were sterilized with ultraviolet (UV) overnight in 24 well plates before the MTT test. After sterilization, they were incubated in DMEM at 37 °C, a 5% CO_2 atmosphere for 30 minutes. After half an hour of incubation, scaffolds were collected and the remaining medium was removed with a micropipette. In the MTT protocol, scaffolds with 1×10^3 hASC (cell/well) were co-cultured for 1, 3, and 7 days at 37 °C, 5% CO_2. To observe the cytotoxic properties of the scaffolds, 10 μg/mL MTT was used, and absorbance was measured at 560 nm. All measurements were repeated with three samples, and mean values were used. In the fixation procedure, the growth medium was removed from the plate, and the scaffolds were fixed with 4% glutaraldehyde to examine the cellular structure on the scaffolds. They were then dehydrated with dilute ethanol. After drying, the scaffolds were coated with Au for 60 seconds and examined under SEM at 10 kV.

After 7 days of cell incubation, cells grown on 40% PMMA and 40% PMMA-based fibers were fixed with 4% formaldehyde for 1 h and then permeabilised with 0.1% Triton X-100 in PBS for 10 min, followed by rinsing with PBS. The samples were incubated with green fluorescent phalloidin conjugate solution for 1 h, followed by nuclear staining with DAPI in the dark. The samples were then placed on glass slides. A confocal laser scanning microscopy (Zeiss LSM700) was used to determine cell fluorescence using a 20 9 oil-immersion objective to obtain images. The samples were examined in confocal microscopy using a green (FITC) channel (Excitation/Emission = 490/525 nm) for F-actin staining and a UV channel (Excitation/Emission = 358/461 nm) for DAPI staining. The Z-stack images of fibers were recorded from top to bottom with a 2.5 μm slice thickness through a depth of ∼ 45 μm.

2.4.7. In vitro drug release behaviors of the drugs from the mat

Firstly, the linear calibration curves of the FCZ and GEN were determined using five different GEN and FCZ concentrations (0.2, 0.4, 0.6, 0.8, and 1 µg/mL). The release behaviors of the GEN and FCZ from the fibers were observed at different time intervals. First of all, 5 mg FCZ and GEN-loaded PMMA fibers were weighed and put into eppendorf tubes with 1 ml PBS ((pH: 7.4). The FCZ and GEN release from the 40% PMMA fibers was performed at a thermal

shaker (BIOSAN TS-100C). The fresh PBS (1 ml) was used during the test. After different time intervals, this 1 ml PBS was taken away from the eppendorf tubes and poured into the quartz bathtub with a 1 ml volume capacity. To detect the absorbance values of the drugs, a UV-Vis spectrophotometer was used at 196 nm and 253 nm wavelengths for GEN and FCZ, respectively. To calculate the cumulative release as a percentage, the absorbance values of the drugs obtained from the release amount detected from different time intervals and the equation in the absorbance graphs obtained from the maximum peak points of the linear calibration curve were used.

Results were presented as mean ± standard error of the mean except for fiber distribution graphs, which were shown as mean ± SD. The pore size was measured using the Image J analysis program. The level of significance was taken $p < 0.05$, and data were labeled with (*) for $p < 0.05$, (**) for $p < 0.01$, (***) for $p < 0.001$.

3. Results and discussions

3.1. Morphological investigations of the electrospun mat

The SEM images of the electrospun fibers are given in Figure 1 with their diameter distributions. Figure 1a represented the SEM image of the 40% PMMA fiber, and it had 2.24 ± 0. 372 µm diameter value. In Figure 1b, by adding 10 mg FCZ into the 40% PMMA, the diameter of the fibers increased to the value of 3.03 ± 0.537 µm. The addition of 10 mg GEN into the 40% PMMA also increased the diameter of the fibers to the value of 3.51 ± 0.76 µm. The diameters of the fibers reached 4.30 ± 1.527 µm with the addition of the drugs combination. The fact that the drugs loaded with 40% PMMA fiber diameter distribution is larger compared to that of 40% PMMA may be due to the noisy contribution of drug molecules placed between polymer chains during fiber formation[23]. According to the SEM images, it can be concluded that the homogeneous, continuous, and beadless morphologies were obtained for all mats. In addition, the images of the drug-loaded mat showed no drug aggregates.

3.2. FTIR analysis

In Figure 2a, the FTIR spectrums of the 40% PMMA had main peaks at 3100-2900 cm^{-1} (CH stretching vibration), 1722.12 cm^{-1} (ester carbonyl group), 1238.08 cm^{-1} (C–O stretching), 950–650 cm^{-1} (C–H bending), and 1145 cm^{-1} to 1271 cm^{-1} (C–O–C stretching vibration)[24]. Figure 2b represented the FTIR spectrums of the fluconazole and the peaks detected at 3200 cm^{-1} (OH stretching, hydroxyl group), 1620 cm^{-1} (C–N stretching, triazole ring). Other peaks found at 1083 and 1112 cm^{-1} pointed out the presence of two kinds of C–F bonds[25]. In Figure 2c, the GEN had principal peaks at 1619 cm^{-1} and 1519 cm^{-1} (NH bending vibrations of primary aromatic amines). Other peaks observed at 1031 and 605 cm^{-1} are due to the sulfur content in the form of an S–O bending vibration and S–O stretch[26]. Figure 2d showed the FTIR spectrum of the 40% PMMA/10 FCZ nanofiber mat. This spectrum was almost similar to the spectrum of the 40% PMMA mat. The FTIR spectrum of the 40% PMMA/10 GEN was given in Figure 2e. This spectrum is also similar to the spectrum of 40% PMMA except for the peak observed at 1675 cm^{-1} which belonged to the pristine GEN. Figure 2f represents the spectrum of the 40% PMMA/10 FCZ/1O GEN mat. The peak at 1677 cm^{-1} also detected the spectrum of the 40% PMMA/10 FCZ/10 GEN mat. According to the results, it was observed that all drug-loaded mat had the same FTIR spectrum with the 40% PMMA, except for some small shifts. The addition of drugs caused small shifts in the main peaks[17]. Since the PMMA has a high amount, all spectrums are nearly the same as the spectrum of the 40% PMMA fiber.

3.3. Thermal behaviors of the fiber mat

3.3.1. DSC analysis

Thermal properties of the fiber mat were investigated, and curves were given in Figure 3. 40% of PMMA had an endothermic peak at 48.23 °C, which was related to the slight weight loss. This mass loss may be associated with the evaporation of the residual solvent (DCM: THF)[27]. The peak detected at 45–50 °C was related to loss of humidity for pristine GEN[28]. The pure FCZ had a sharp peak at 140 °C which was due to the melting of FCZ, and a small peak around 27 °C which is related to initial heating[29]. The DSC curves of 40% PMMA/10 FCZ, 40% PMMA/10 GEN, and 40% PMMA/10 FCZ/10 GEN had the same thermal points compared to the curve of 40% PMMA. This showed that there was no significant change in the heat flow properties between the 40% PMMA and drug-loaded 40% PMMA fiber mat[30].

3.3.2. TGA analysis

Table 1 demonstrated the 5% weight loss temperature values of the 40% PMMA, 40% PMMA/10 FCZ, 40% PMMA/10 GEN, and 40% PMMA/10 FCZ/10 GEN fiber mat. By adding 10 mg FCZ into the 40% PMMA fiber, the 5% weight loss temperature value shifted from 32.62 °C to 27.93 °C. On the other hand, 10 mg GEN addition increased the 32.62 °C to 33.67 °C. The combination of the two drugs together lost 5% of mass at 30.45 °C. As a result of TGA, it can be said that the addition of FCZ negatively affected the thermal stability, but the addition of GEN increased the thermal stability.

3.4. Tensile testing results of the fiber mat

Table 2 shows the stress-strain behavior of the 40% PMMA, 40% PMMA/10 FCZ, 40% PMMA/10 GEN, and 40% PMMA/10 FCZ/10 GEN fibers. When the results were examined, it was seen that the 40% PMMA had a tensile strength of 0.354 MPa and a tensile strain value of 0.749%. With the addition of 10 mg of FCZ, the tensile strength of

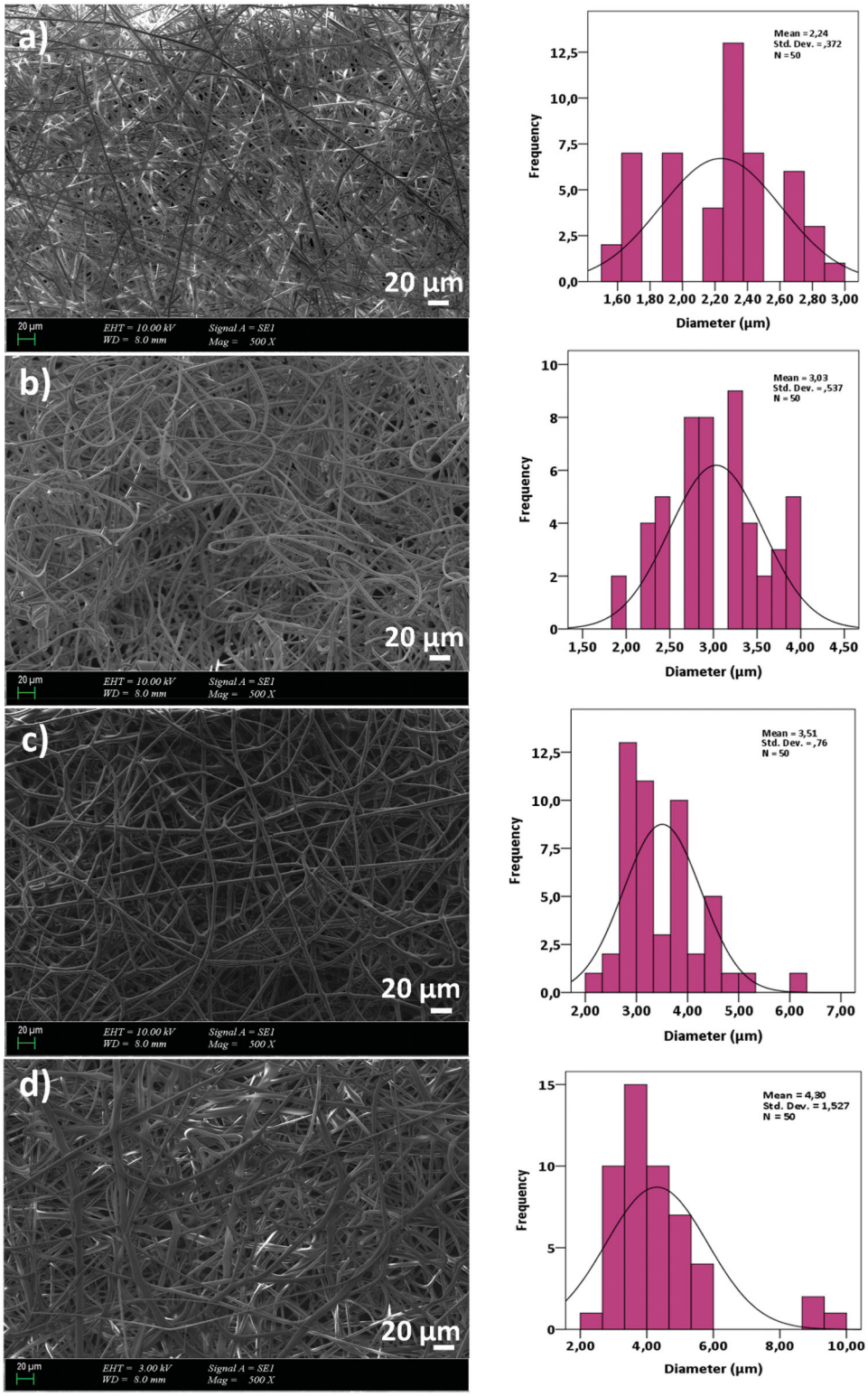

Figure 1. SEM images of the 40% PMMA (a), 40% PMMA/10 FCZ (b), 40% PMMA/10 GEN (c), and 40% PMMA/10 FCZ/10 GEN (d) fibers.

PMMA decreased to 0.0842 MPa, and the elongation decreased to 0.334%. The decrease in mechanical strength with FCZ addition may be due to an increase in the number of stress points that amount to the existence of drug particles in the fiber mat[31]. On the other hand, with the addition of 10 mg GEN into 40% PMMA fiber, the tensile strength increased to 1.4885 MPa, and the elongation amount was found to be 0.491%. The tensile strength of the nanofibers obtained by adding 10 mg FCZ and 10 mg GEN into 40% PMMA was found to be 1.211 MPa and the elongation amount was 0.382%. According to the results, it can be said that the addition of FCZ reduced the tensile strength and elongation amount, while the addition of GEN increased the mechanical strength. In addition, the tensile

strength of drug combinations was higher than 40% PMMA in the control group. The improved mechanical strength can be due to the efficient load transfer from polymer matrices to the GEN[32].

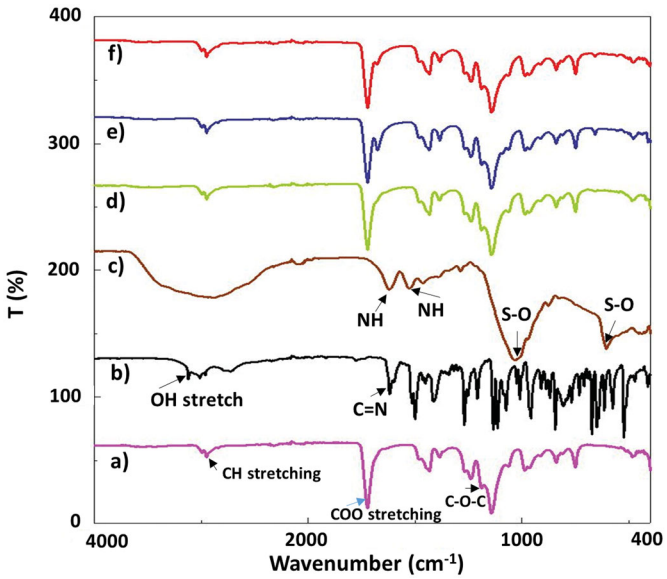

Figure 2. FTIR spectrums of the 40% PMMA (a), pure FCZ (b), pure GEN (c), 40% PMMA/10 FCZ (d), 40% PMMA/10 GEN (e), and 40% PMMA/10 FCZ/10 GEN (f).

3.5. Evaluation of antimicrobial properties of the GEN-loaded fiber mat

The antimicrobial activity of the samples is a significant element in wound healing performance. Bacterial activity on the wound surface causes inflammation and infection and produces toxic metabolites that delay healing[33]. The antimicrobial activity results of the mat were given in Figure 4 and Table 3. The fiber mat was tested against *P. aeruginosa* (ATCC 27853), *S. aureus* (ATCC 29213), *S. pneumoniae* (ATCC 49619), *C. albicans* (SC53149), and *C. parapsilosis* (ATCC 22019). When the results were examined, it was observed that FCZ added fibers did not have antimicrobial activity against the bacterial and fungal strains. This may be due to the amounts of FCZ, or the widespread usage of FCZ, which can cause the resistance of bacterial and fungal strains against this drug[34].

On the other hand, GEN addition enhanced the antibacterial activity of the 40% PMMA fibers against the *P. aeruginosa* and *S. aureus* with 10 mm and 16 mm inhibition zones, respectively. However, GEN addition fibers did not show any antifungal activity. When the antimicrobial activity results of the 40% PMMA/10 FCZ/10 GEN fibers were examined, it was observed that they formed inhibition diameters of 12 and 10 mm against the *S. aureus* and *P. aeruginosa*, respectively. *S. aureus* and *P. aeruginosa* is a familiar cause of ocular infections[35,36]. Therefore, it is essential to provide antimicrobial activity to the fibers to treat ocular infections such as keratitis.

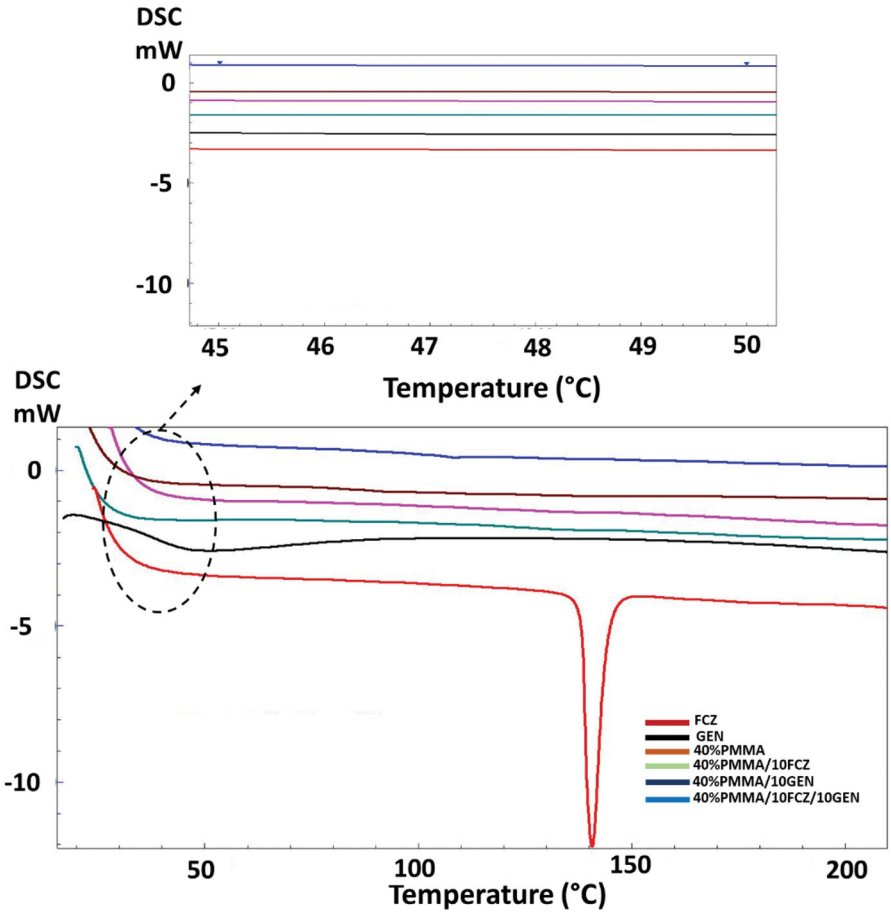

Figure 3. DSC curves of the pure FCZ, GEN, and PMMA-based blends.

Table 1. 5% Weight loss temperature values of the fiber mat.

Fibers	5% Weight loss temperatures (°C)
40% PMMA	32.62
40% PMMA/10 FCZ	27.93
40% PMMA/10 GEN	33.67
40% PMMA/10 FCZ/10 GEN	30.45

Table 2. Tensile properties of the fiber mat.

Fiber mat	Tensile strength (MPa)	Strain at break (%)
40% PMMA	0.354 ± 0.069	0.749 ± 0.022
40% PMMA/10 FCZ	0.0842 ± 0.027	0.334 ± 0.058
40% PMMA/10 GEN	1.4885 ± 0.288	0.491 ± 0.05
40% PMMA/10 FCZ/10 GEN	1.211 ± 0.331	0.382 ± 0.203

The values given in Table 2 are the mean values of the three replicates for each mat.

3.6. MTT assay, cell distribution on the fiber mat, and cell migration

Figure 5 shows the MTT assay results of the scaffolds after 1, 3, and 7 days of incubation with MSCs. When the viability amounts on the first day were examined, it was found that the highest percentage of viability belonged to 40% PMMA (89.7%) and 10 GEN (88.4%) fibers. The lowest cell viability (56.1%) belonged to fiber-containing FCZ. On the third day, viability values increased significantly in all samples except 40% PMMA fiber. 40% PMMA fiber has 59.7% cell viability. However, on day 7, the viability value for 40% PMMA increased again and reached 88.6%. The viability values of 40% PMMA/10 FCZ and 40% PMMA/10 GEN fibers decreased on the 7th day. On the other hand, the number of cells in the samples containing 40% PMMA/10 FCZ/10 GEN reached its

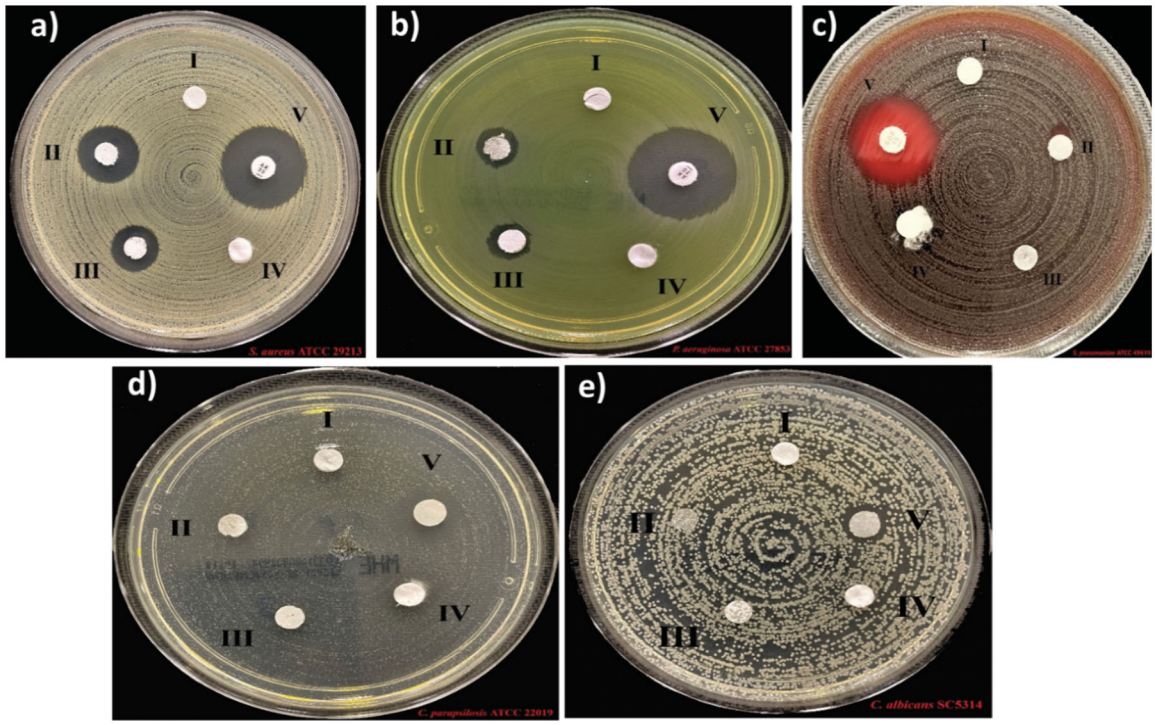

Figure 4. Antimicrobial activity results from the fiber mat against the *S. aureus* (a), *P. aeruginosa* (b), *S. pneumoniae* (c), *C. parapsilosis* (d), and *C. albicans* (e). The fiber mat was labeled as 40% PMMA/10 FCZ (I), 40% PMMA/10 GEN (II), 40% PMMA/10 FCZ/10 GEN (III), and 40% PMMA (IV). Control groups (Amikacin for *S. aureus* and *P. aeruginosa,* norfloxacin for *S. pneumoniae,* ethanol for *C. albicans,* and *C. parapsilosis)* were labeled as V.

Table 3. The inhibition zone values of the samples against the microbics.

Samples	*P. aeruginosa* ATCC 27853 Inhibition zone (mm)	*S. aureus* ATCC 29213 Inhibition zone (mm)	*S. pneumoniae* ATCC 49619 Inhibition zone (mm)	*C. albicans* SC5314 Inhibition zone (mm)	*C. parapsilosis* ATCC 22019 Inhibition zone (mm)
40% PMMA/10 FCZ (I)	0	0	0	0	0
40% PMMA/10 GEN (II)	10	16	0	0	0
40% PMMA/10 FCZ/1O GEN (III)	10	12	0	0	0
40% PMMA (IV)	0	0	0	0	0
Amikacin (V) (AMK, 30 μg)	24	22	–	–	–
Norfloxacin (V) (NOR, 10 μg)	–	–	23	–	–
Ethanol (V) (70%)	–	–	–	11	11

maximum on the 7th day and surpassed the control group (2 D) (103.9%). In Khodir et al.'s study, they fabricated gentamicin added Polycaprolactone (PCL)/Collagen (COL) nanofibers for skin tissue engineering. Biocompatibility properties of the fibers were tested with a human dermal fibroblast (HDF) stem cell line. According to the result, gentamicin loaded nanofibers promoted cell growth and attachment[23].

Cell attachment and proliferation were observed on the surface of the 40% PMMA, 40% PMMA/10 FCZ, 40% PMMA/10 GEN, and 40% PMMA/10 FCZ/10 GEN fibers, as shown in Figure 6. There was no significant difference in the average cell densities of the 40% PMMA and 40% PMMA/10 FCZ, 40% PMMA/10 GEN, 40% PMMA/10 FCZ/10 GEN groups for the first day of incubation time. The cell

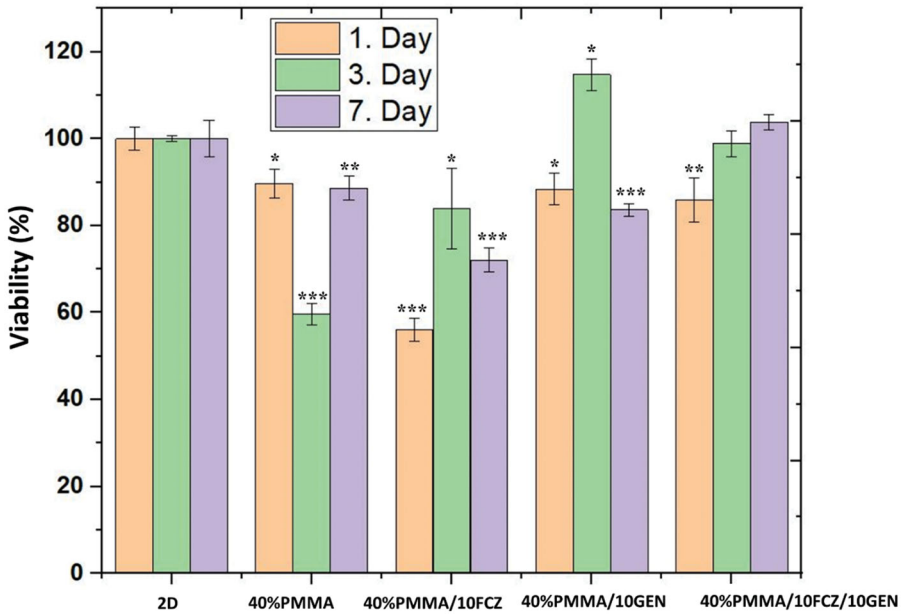

Figure 5. The proliferation of MSCs on the fiber mat after 1, 3, and 7 days of incubation.

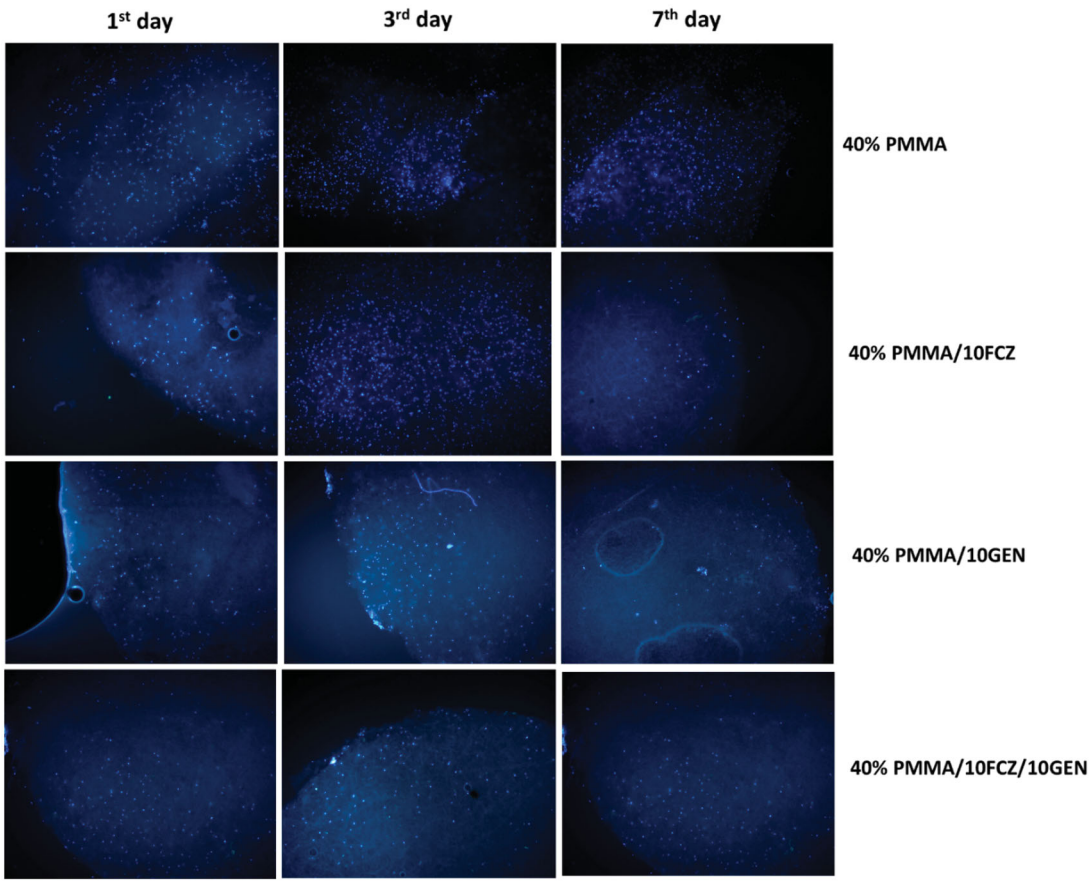

Figure 6. MSCs viability on the fiber mat after 1, 3, and 7 days of the culture period.

distributions on the fibers increased for 40% PMMA and 40% PMMA/10 FCZ fibers, and the cell distributions on the 40% PMMA/10 GEN and 40% PMMA/10 FCZ/10 GEN stayed nearly the same after 3 days of culture time. According to the cell distribution results on the 7th day, it was observed that the cell density on the 40% PMMA fiber increased, while the mean percentage of cells on the other fibers decreased compared to the results of the 1st and 3rd days.

On the 7th day of the incubation, the morphologies and attachment of the MSCs on the fiber mat were examined with SEM in Figure 7. Characteristic MSC morphologies were detected on the fibers. It was observed that cells attached to the surface of the fibers and distributed on the fibers with their filopodia[27].

Figure 8 shows the Z-stack images and the reconstructed 3 D projection image obtained from the surface to the underside of a 40% PMMA-based fiber mat with a 2.5 µm slice thickness. As shown in Figure 8, optical slicing in the Z-direction using Z-stack optical confocal microscopy allowed us to observe the penetration of cells into a 40% PMMA-based fiber mat. Cells were observed to infiltrate the scaffold at a depth of 45 µm from the top surface of the scaffold. These results demonstrate successful growth, proliferation, and infiltration of the cytoskeleton within fibers, demonstrating their suitability for cell-cell and cell-matrix interactions *in vitro*.

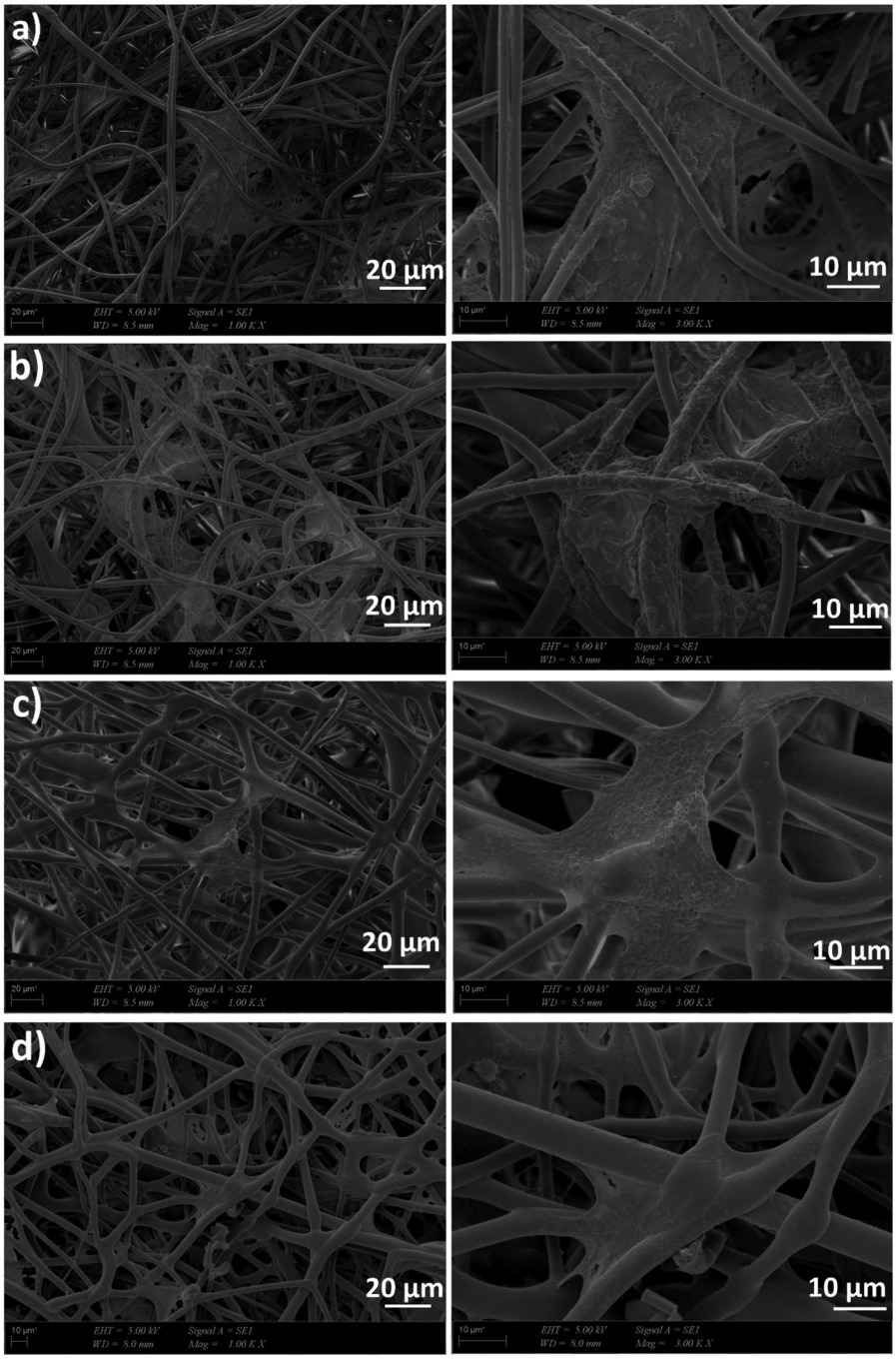

Figure 7. SEM micrographs of MSCs cultured on culture slide containing 40% PMMA (a), 40% PMMA/10 FCZ (b), 40% PMMA/10 GEN (c), and 40% PMMA/10 FCZ/10 GEN (d).

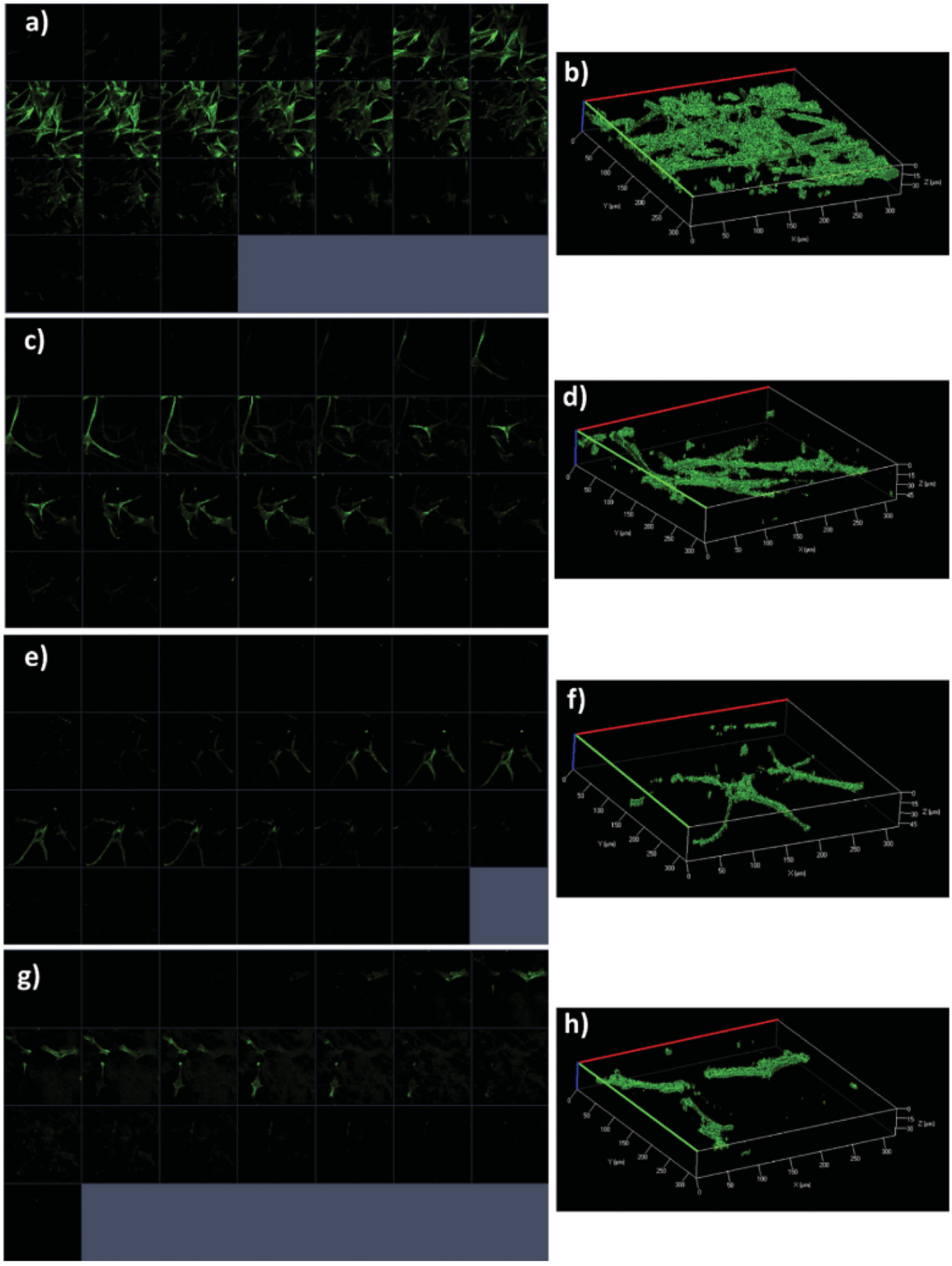

Figure 8. The Z-stack images of optical confocal images from top to bottom with a 2.5 μm slice thickness and the reconstructed 3 D projection image of the fiber mat; 40% PMMA (a, b), 40% PMMA/10 FCZ (c, d), 40% PMMA/10 GEN (e, f), and 40% PMMA/10 FCZ/10 GEN (g, h).

3.7. In vitro *release study of FCZ and GEN*

The FCZ and GEN release behaviors were investigated in PBS at a thermal shaker, and the results are given in Figure 9. Figure 9a represents the calibration curve determined with five different solutions (0.2, 0.4, 0.6, 0.8, and 1 μg/mL), and Figure 9b shows the absorbance graph obtained from the calibration curve at 253 nm and 196 nm for FCZ and GEN, respectively. Figure 9c shows the cumulative release graph of the FCZ from the fiber mat. According to the graph, in the first 15 minutes, the release percentage reached 21.71%. After half an hour, the percentage of release reached 39.22%. After an hour, approximately 56.87% of the FCZ was released. All the FCZ into the fibers was released within 24 hours. According to the results, there was observed

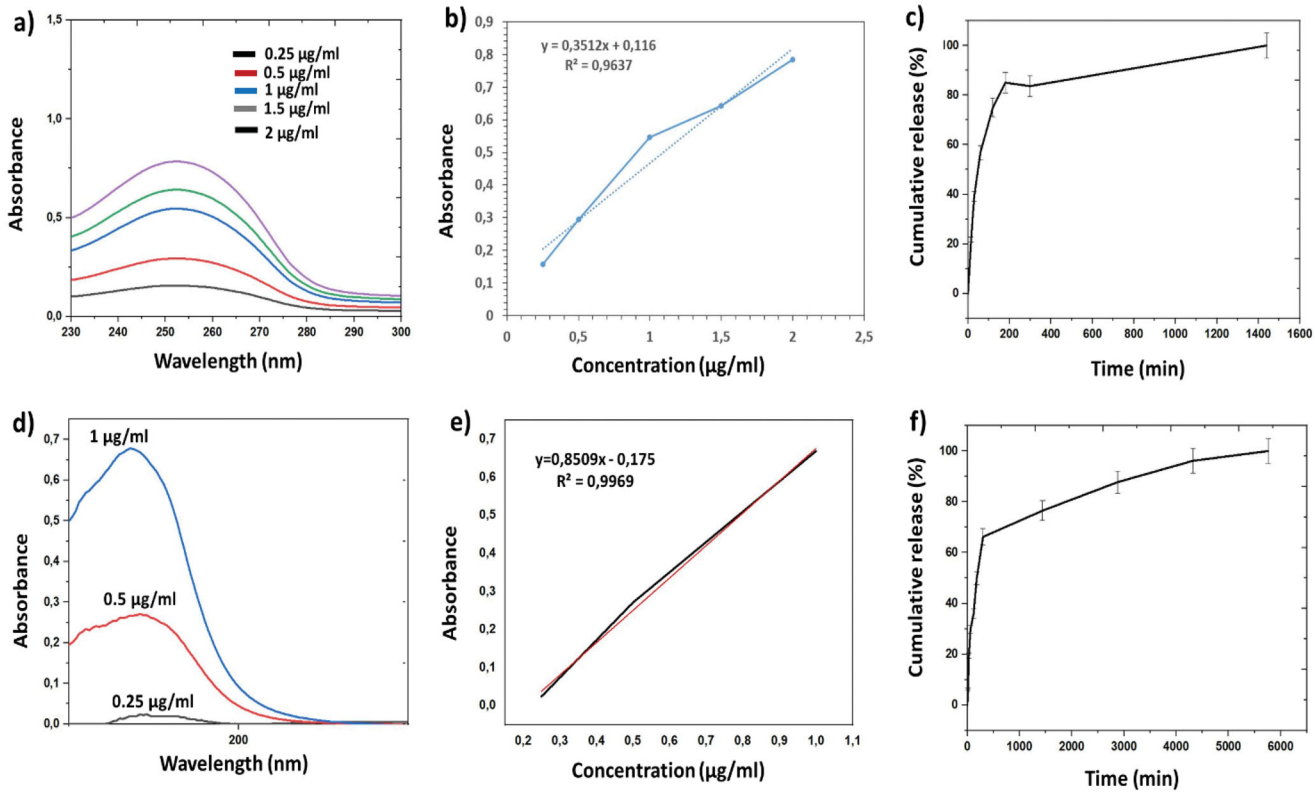

Figure 9. The linear calibration curves of the FCZ (a) and GEN (d), absorbance graphs of the FCZ (b) and GEN (e) obtained from calibration curves, and the cumulative release profiles of the FCZ (c) and GEN (f) from the fiber mat.

a rapid release of FCZ from fibers (56.87% in the first hour). In the fluconazole release test, it was observed that the release was rapid at the beginning of the release due to the high specific surface area of the fibers and the presence of the drug on the fiber surface[37]. Figure 9f belonged to the cumulative release graph of the GEN. In the first 15 minutes, the release amount of the GEN reached the 6.31% value. After half an hour, 19.53% release amount was detected, and within an hour, this value reached 29.81%. The GEN reached a release value of ~50% at the 3rd hour. After the third hour, the amount of release increased, and by the fourth day, all drug was completely released from the fibers. As a result, it can be concluded that in the 40% PMMA/10 FCZ/10 GEN fiber mat, firstly, FCZ can release quickly from the mat, and GEN also can begin to release but takes a longer time compared to the FCZ. However, according to the antimicrobial test, even if FCZ is released first and more, it will not be beneficial because it is ineffective against bacteria. With the release of the GEN, defence against bacteria will be possible.

4. Conclusions

In this research, 40% of PMMA fiber mats were successfully fabricated using the electrospinning process. FCZ and GEN were loaded into this fiber to provide antimicrobial activity against the *P. aeruginosa*, *S. aureus*, *S. pneumoniae*, *C. albicans*, and *C. parapsilosis,* which are the common microorganisms that generate corneal keratitis. FCZ and GEN were used as antifungal and antibacterial agents, respectively. According to the SEM images, it can be concluded that the diameters of the fibers increased with drug addition. Thermal characterizations showed that drug addition did not change the specific thermal points of the PMMA. Antimicrobial activity results showed that 40% PMMA/10 FCZ did not show antibacterial and antifungal activities. However, GEN addition provided the antibacterial activity to the 40% PMMA/10 GEN and 40% PMMA/10 FCZ/10 GEN fibers. According to the tensile test, results demonstrated that GEN addition enhanced the mechanical strength of the fiber mat and FCZ addition decreased this property. The drug release results indicated that FCZ was released more rapidly from the fibers than GEN. Cell culture experiments reported that the 40% PMMA/10 GEN and 40% PMMA/10 FCZ/10 GEN fibers showed good biocompatibility with MSCs and great potential for treating corneal keratitis.

Acknowledgments

The authors thank Ecem Dogan, Dr. Semra Unal, Dr. Mehmet Mucahit Guncu, Dr. Burak Aksu, and Dr. Ali Sahin for antimicrobial and biocompatibility tests.

Data availability statement

The raw data will be made available upon request.

References

[1] Copeland, R. A.; Davis, S. A.; Lee, Y. J.; Kwagyan, J.; Bovelle, R. Corneal Collagen Cross-Linking for Infectious Keratitis. *Cochrane Database Syst. Rev.* **2018**, *2018*, 62–71.

[2] Ulag, S.; Ilhan, E.; Demirhan, R.; Sahin, A.; Karademir Yilmaz, B.; Aksu, B.; Sengor, M.; Ficai, D.; Titu, A. M.; Ficai, A.; Gunduz, O. Propolis-Based Nanofiber Mat to Repair Corneal Microbial Keratitis. *Molecules.* **2021**, *26*, 2577. DOI: 10.3390/molecules26092577.

[3] Ulag, S.; Ilhan, E.; Aksu, B.; Sengor, M.; Ekren, N.; Kilc, O.; Gunduz, O. Patch-Based Technology for Corneal Microbial Keratitis. Bioinformatics and Biomedical Engineering: 8th International Work-Conference, IWBBIO 2020, Granada, Spain, May 6–8, 2020. DOI: 10.1007/978-3-030-45385-5_18.

[4] Vajpayee, R. B.; Dada, T.; Saxena, R.; Vajpayee, M.; Taylor, H. R.; Venkatesh, P.; Sharma, N. Study of the First Contact Management Profile of Cases of Infectious Keratitis: A Hospital-Based Study. *Cornea.* **2000**, *19*, 52–56. DOI: 10.1097/00003226-200001000-00011.

[5] Dart, J. K. G. Predisposing Factors in Microbial Keratitis: The Significance of Contact Lens Wear. *Br. J. Ophthalmol.* **1988**, *72*, 926–930. DOI: 10.1136/bjo.72.12.926.

[6] Schaefer, F.; Bruttin, O.; Zografos, L.; Guex-Crosier, Y. Bacterial Keratitis: A Prospective Clinical and Microbiological Study. *Br. J. Ophthalmol.* **2001**, *85*, 842–847. DOI: 10.1136/bjo.85.7.842.

[7] Mackool, R. Microbial Keratitis following Corneal Transplantation. *Am. J. Ophthalmol.* **2007**, *143*, 910. DOI: 10.1016/j.ajo.2007.02.018.

[8] Upadhyay, M. P.; Srinivasan, M.; Whitcher, J. P. Diagnosing and Managing Microbial Keratitis. *Community Eye Heal. J.* **2015**, *28*, 3–6.

[9] Martin, R. F.; Murray, V.; D'Cunha, G.; Pardee, M.; Kampouris, E.; Haigh, A.; Kelly, D. P.; Hodgson, G. S. Radiation Sensitization by an Iodine-Labelled DNA Ligand. *Int. J. Radiat. Biol.* **1990**, *57*, 939–946. DOI: 10.1080/09553009014551061.

[10] Strieter, R. M.; Kunkel, S. L.; Elner, V. M.; Martonyi, C. L.; Koch, A. E.; Polverini, P. J.; Elner, S. G. Interleukin-8: A Corneal Factor That Induces Neovascularization. *Am. J. Pathol.* **1992**, *141*, 1279–1284.

[11] Matthews, T. D.; Frazer, D. G.; Minassian, D. C.; Radford, C. F.; Dart, J. K. G. Risks of Keratitis and Patterns of Use with Disposable Contact Lenses. *Arch. Ophthalmol.* **1992**, *110*, 1559–1562. DOI: 10.1001/archopht.1992.01080230059020.

[12] Shah, R.; Shah, M.; Khandekar, R.; Al-raisi, A. Contact Lens Induced Corneal Ulcer Management in Tertiary Eye Unit in Oman – A Descriptive Study. *Sultan Qaboos Univ. Med. J.* **2020**, *8*, 283–290.

[13] Ormerod, L. D.; Hertzmark, E.; Gomez, D. S.; Stabiner, R. G.; Schanzlin, D. J.; Smith, R. E. Epidemiology of Microbial Keratitis in Southern California. A multivariate analysis. *Ophthalmology.* **1987**, *94*, 1322–1333. DOI: 10.1016/S0161-6420(87)80019-2.

[14] Pakzad-Vaezi, K.; Levasseur, S. D.; Schendel, S.; Mark, S.; Mathias, R.; Roscoe, D.; Holland, S. P. The Corneal Ulcer One-Touch Study: A Simplified Microbiological Specimen Collection Method. *Am. J. Ophthalmol.* **2015**, *159*, 37–43.e1. DOI: 10.1016/j.ajo.2014.09.021.

[15] Mobaraki, M.; Abbasi, R.; Omidian Vandchali, S.; Ghaffari, M.; Moztarzadeh, F.; Mozafari, M. Corneal Repair and Regeneration: Current Concepts and Future Directions. *Front. Bioeng. Biotechnol.* 2019, *7*, 135. DOI: 10.3389/fbioe.2019.00135.

[16] Essam, T. *Dual Drug-Loaded Electrospun Nanofibres for the Treatment of Corneal Diseases.* University College London School of Pharmacy: London, UK, 2019.

[17] Cesur, S.; Ulag, S.; Ozak, L.; Gumussoy, A.; Arslan, S.; Yilmaz, B. K.; Ekren, N.; Agirbasli, M.; kalaskar, D. M.; Gunduz, O. Production and Characterization of Elastomeric Cardiac Tissue-like Mat for Myocardial Tissue Engineering. *Polym. Test.* **2020**, *90*, 106613. DOI: 10.1016/j.polymertesting.2020.106613.

[18] Croitoru, A.-M.; Karaçelebi, Y.; Saatcioglu, E.; Altan, E.; Ulag, S.; Aydoğan, H. K.; Sahin, A.; Motelica, L.; Oprea, O.; Tihauan, B.-M.; et al. Electrically Triggered Drug Delivery from Novel Electrospun Poly (Lactic Acid)/Graphene Oxide/Quercetin Fibrous Scaffolds for Wound Dressing Applications. *Pharmaceutics.* **2021**, *13*, 957. DOI: 10.3390/pharmaceutics13070957.

[19] Isha, A.; Yusof, N. A.; Ahmad, M.; Suhendra, D.; Yunus, W. M. Z. W.; Zainal, Z. A Chemical Sensor for Trace V(V) ion Determination Based on Fatty Hydroxamic Acid Immobilized in Polymethylmethacrylate. *Sensors Actuators B Chem.* **2006**, *114*, 344–349. DOI: 10.1016/j.snb.2005.06.007.

[20] Mishra, S.; Sen, G. Microwave Initiated Synthesis of Polymethylmethacrylate Grafted Guar (GG-g-PMMA), Characterizations and Applications. *Int. J. Biol. Macromol.* **2011**, *48*, 688–694. DOI: 10.1016/j.ijbiomac.2011.02.013.

[21] Amer, Z. J. A.; Ahmed, J. K.; Abbas, S. F. Chitosan/PMMA Bioblend for Drug Release Applications. *Int. J. Eng. Technol* **2014**, *4*, 318–324.

[22] Pinar,] E.; Sahin, A.; Unal, S.; Gunduz, O.; Harman, F.; Kaptanoglu, E. The Effect of Polycaprolactone/Graphene Oxide Electrospun Scaffolds on the Neurogenic Behavior of Adipose Stem Cells. *Eur. Polym. J.* **2022**, *165*, 111000. DOI: 10.1016/j.eurpolymj.2022.111000.

[23] Khodir, W. K. W. A.; Abdul Razak, A. H.; Ng, M. H.; Guarino, V.; Susanti, D. Encapsulation and Characterization of Gentamicin Sulfate in the Collagen Added Electrospun Nanofibers for Skin Regeneration. *JFB.* **2018**, *9*, 36. DOI: 10.3390/jfb9020036.

[24] Piperno, S.; Lozzi, L.; Rastelli, R.; Passacantando, M.; Santucci, S. PMMA Nanofibers Production by Electrospinning. *Appl. Surf. Sci.* **2006**, *252*, 5583–5586. DOI: 10.1016/j.apsusc.2005.12.142.

[25] Ghosh, M.; Mandal, S.; Roy, A.; Chakrabarty, S.; Chakrabarti, G.; Kumar Pradhan, S. Enhanced Antifungal Activity of Fluconazole Conjugated with Cu-Ag-ZnO Nanocomposite. *Mater Sci Eng C Mater Biol Appl* **2020**, *106*, 110160. DOI: 10.1016/j.msec.2019.110160.

[26] Mosselhy, D. A.; He, W.; Hynönen, U.; Meng, Y.; Mohammadi, P.; Palva, A.; Feng, Q.; Hannula, S.-P.; Nordström, K.; Linder, M. B. Silica-Gentamicin Nanohybrids: Combating Antibiotic Resistance, Bacterial Biofilms, and *In Vivo* Toxicity. *Int. J. Nanomedicine.* **2018**, *13*, 7939–7957. DOI: 10.2147/IJN.S182611.

[27] Ulag, S.; Sahin, A.; Guncu, M. M.; Aksu, B.; Ekren, N.; Sengor, M.; Kalaskar, D. M.; Gunduz, O. A Novel Approach to Treat the Thiel-Behnke Corneal Dystrophy Using 3D Printed Honeycomb-Shaped Polymethylmethacrylate (PMMA)/Vancomycin (VAN) Scaffolds. *Bioprinting.* **2021**, *24*, e00173. DOI: 10.1016/j.bprint.2021.e00173.

[28] Shiehzadeh, F.; Tafaghodi, M.; Laal-Dehghani1, M.; Mashhoori1, F.; Sedigheh, B.; Bazzaz, F.; Imenshahidi, M. Preparation and Characterization of a Dry Powder Inhaler Composed of PLGA Large Porous Particles Encapsulating Gentamicin Sulfate. *Adv. Pharm. Bull.* **2019**, *9*, 255–261. DOI: 10.15171/apb.2019.029.

[29] Desai, S. R.; Shaikh, M. M.; Dharwadkar, S. R. Thermoanalytical Study of Polymorphic Transformation in Fluconazole Drug. *Thermochim. Acta.* **2003**, *399*, 81–89. DOI: 10.1016/S0040-6031(02)00451-3.

[30] Thomas, P.; Ernest Ravindran, R. S.; Varma, K. Structural, Thermal and Electrical Properties of Poly(Methyl Methacrylate)/CaCu3Ti4O12 Composite Sheets Fabricated via Melt Mixing. *J. Therm. Anal. Calorim.* **2014**, *115*, 1311–1319. DOI: 10.1007/s10973-013-3500-x.

[31] Sharma, R.; Garg, T.; Goyal, A. K.; Rath, G. Development, Optimization and Evaluation of Polymeric Electrospun Nanofiber: A Tool for Local Delivery of Fluconazole for Management of Vaginal Candidiasis. *Artif. Cells Nanomed. Biotechnol.* **2016**, *44*, 524–531. DOI: 10.3109/21691401.2014.966194.

[32] Wali, A.; Gorain, M.; Inamdar, S.; Kundu, G.; Badiger, M. In Vivo Wound Healing Performance of Halloysite Clay and

Gentamicin-Incorporated Cellulose Ether-PVA Electrospun Nanofiber Mats. *ACS Appl. Bio. Mater.* **2019**, *2*, 4324–4334. DOI: 10.1021/acsabm.9b00589.

[33] Hajikhani, M.; Emam-Djomeh, Z.; Askari, G. Fabrication and Characterization of Mucoadhesive Bioplastic Patch via Coaxial Polylactic Acid (PLA) Based Electrospun Nanofibers with Antimicrobial and Wound Healing Application. *Int. J. Biol. Macromol.* **2021**, *172*, 143–153. DOI: 10.1016/j.ijbiomac.2021.01.051.

[34] Shirinzadeh, H.; Süzen, S.; Altanlar, N.; Westwell, A. D. Antimicrobial Activities of New Indole Derivatives Containing 1,2,4-Triazole, 1,3,4-Thiadiazole and Carbothioamide. *Turk. J. Pharm. Sci.* **2018**, *15*, 291–297.

[35] Mirzaeei, S.; Barfar, D. Design and Development of Antibacterial/anti-Inflammatory Dual Drug-Loaded Nanofibrous Inserts for Ophthalmic Sustained Delivery of Gentamicin and Methylprednisolone: *In Vitro* Bioassay, Solvent, and Method Effects' Evaluation. *Adv. Pharm. Bullet*. 2021. DOI: 10.34172/apb.2022.056

[36] Hilliam, Y.; Kaye, S.; Winstanley, C. Pseudomonas aeruginosa and Microbial Keratitis. *J. Med. Microbiol.* **2020**, *69*, 3–13. DOI: 10.1099/jmm.0.001110.

[37] Semnani, D.; Afrashi, M.; Alihosseini, F.; Dehghan, P.; Maherolnaghsh, M. Investigating the Performance of Drug Delivery System of Fluconazole Made of Nano–Micro Fibers Coated on Cotton/Polyester Fabric. *J. Mater. Sci: Mater. Med.* **2017**, *28*, 175. DOI: 10.1007/s10856-017-5957-9.